

Transition between free, mixed and forced convection

**W Jaeger^{1,6}, F Trimborn^{3,5}, M Niemann⁴, V Saini^{4,5}, W Hering², R Stieglitz²,
B Pritz³, J Fröhlich⁴ and M Gabi³**

¹Institute of Fusion and Reactor Technology, Karlsruhe Institute of Technology (KIT),
Kaiserstraße 12, 76131 Karlsruhe, Germany

²Institute for Neutron Physics and Reactor Technology, Karlsruhe Institute of
Technology (KIT), Hermann-von-Helmholtz-Platz 1, 76344 Eggenstein-
Leopoldshafen, Germany

³Institute of Fluid Machinery, Karlsruhe Institute of Technology (KIT),
Kaiserstraße 12, 76131 Karlsruhe, Germany

⁴Institute of Fluid Mechanics, Technische Universität Dresden, 01062 Dresden,
Germany

⁵Currently at: Laboratoire de Mécanique de Lille, Ecole Central de Lille, Boulevard
Paul Langevin, 59655 Villeneuve d'Ascq Cédex, France

⁶wadim.jaeger@kit.edu

Abstract. In this contribution, numerical methods are discussed to predict the heat transfer to liquid metal flowing in rectangular flow channels. A correct representation of the thermo-hydraulic behaviour is necessary, because these numerical methods are used to perform design and safety studies of components with rectangular channels. Hence, it must be proven that simulation results are an adequate representation of the real conditions. Up to now, the majority of simulations are related to forced convection of liquid metals flowing in circular pipes or rod bundle, because these geometries represent most of the components in process engineering (e.g. piping, heat exchanger). Open questions related to liquid metal heat transfer, among others, is the behaviour during the transition of the heat transfer regimes. Therefore, this contribution aims to provide useful information related to the transition from forced to mixed and free convection, with the focus on a rectangular flow channel. The assessment of the thermo-hydraulic behaviour under transitional heat transfer regimes is pursued by means of system code simulations, RANS CFD simulations, LES and DNS, and experimental investigations. Thereby, each of the results will be compared to the others. The comparison of external experimental data, DNS data, RANS data and system code simulation results shows that the global heat transfer can be consistently represented for forced convection in rectangular flow channels by these means. Furthermore, LES data is in agreement with RANS CFD results for different Richardson numbers with respect to temperature and velocity distribution. The agreement of the simulation results among each other and the hopefully successful validation by means of experimental data will foster the confidence in the predicting capabilities of numerical methods, which can be applied to engineering application.



1. Introduction

Liquid metal flows are characterized by low molecular Prandtl numbers, which strongly influence the transport of heat from solid surfaces. As a result, they are capable to transfer quantities of thermal energy at low temperature differences to a large fraction by molecular diffusion. This allows operating thermodynamic processes on higher temperature levels attaining potentially higher overall efficiencies of the whole system. In order to optimize the design or evaluate the performance of such large scale facilities, local predictions are required. For the latter reliable experimental data are lacking, and hence one strategy is to obtain data from direct or partially resolved numerical simulations (DNS or LES) or data from simulations based on the Reynolds-averaged Navier-Stokes equations (RANS). Within the scope of the latter numerical methods, the RANS approach still seems to be the best compromise between required numerical effort and accuracy among the given methods, because the realization of DNS or even LES is still limited to rather simple geometries and specialized numerical codes. Experiments in liquid metals require a detailed knowledge of handling low molecular Prandtl number fluids. Safety aspects, purity of the material and chemical reactivity, e.g. the reactivity of liquid sodium or steel corrosion in Lead-Bismuth Eutectic (LBE) must be taken into account. The simultaneous measurement of local mean and fluctuating quantities with high accuracy and resolution to validate numerical methods is a further challenge. Detailed accounts on low Prandtl number thermal-hydraulics and related measurements can be found in the most recent publications of [1][2][3].

This article addresses this aspect. Because the usual approach based on a similarity assumption between the turbulent eddy viscosity and the turbulent thermal diffusivity leads to inaccurate results, more sophisticated turbulent heat flux models are developed, and their results are analyzed for validation purposes. Especially with respect to different convection regimes (forced, mixed and natural convection) and the transition from one regime to the other, the modelling of the turbulent heat fluxes has to incorporate the thermal-hydraulic peculiarities of liquid metal flows. Furthermore, the flow in a rectangular channel is characterized by the occurrence of the well-known secondary motions of the second kind, which show a notable impact on the heat transfer of already in higher Prandtl number flows. Thus, anisotropic modelling approaches for the closure of the turbulent momentum equations have to be investigated to provide an accurate basis for further modelling activities and investigations. Thereby, the subjects of the described task can be linked to the contributing organizations: Coordination and development of the experiment – KIT; Turbulent heat flux analysis by means of RANS CFD and LES – KIT; LES and DNS – TU Dresden.

2. Turbulent heat flux modelling

2.1. Analysis of the budget terms of turbulent heat fluxes

To account for most of the features and requirements of turbulent heat transfer in liquid metal flows, second-moment closures for the turbulent heat fluxes, based on the solution of three additional transport equations, seem to be the natural choice. This requires a detailed analysis of the main transport and destruction mechanisms of turbulent heat fluxes in dependence of the molecular Prandtl number Pr ($Pr = \eta \cdot c_p / k$), the Reynolds number ($Re = \rho \cdot u \cdot d / \eta$) and the Péclet number ($Pe_b = Pr \cdot Re_b$). The full transport equation of the turbulent heat fluxes $\overline{u_i \theta}$ in symbolic notation is given by:

$$\frac{\mathbf{D} \overline{u_i \theta}}{\mathbf{D} t} = P_{i\theta} + \Pi_{i\theta} + D_{i\theta}^v + D_{i\theta}^t - \varepsilon_{i\theta}, \quad (1)$$

where $P_{i\theta}$ represents the production of turbulent heat fluxes due to the mean flow, $\Pi_{i\theta}$ the temperature-pressure gradient correlation, $D_{i\theta}^v$ and $D_{i\theta}^t$ the molecular and turbulent diffusion and $\varepsilon_{i\theta}$ the dissipation term. The production term $P_{i\theta}$ needs no further modelling, which is one of the most important advantages of this level of closure. Each of the other terms, even the molecular diffusion term, needs further modelling strategies. The correlation term $\Pi_{i\theta}$ is often divided into the pressure-scrambling term $\phi_{i\theta}$ and the pressure diffusion term $D_{i\theta}^p$, which is only of minor importance far away from the wall in duct flows and therefore usually absorbed into the modelling of the turbulent diffusion term $D_{i\theta}^t$. To

identify the behaviour of the main budget terms for different frictional Reynolds and Prandtl numbers, the DNS data by Abe et al. [4] are used; see Figure 1. Thereby, the frictional Reynolds number (Re_τ) is based on the frictional velocity u_τ .

For Prandtl numbers near unity, the correlation term $\Pi_{i\theta}$ is the main counterpart of the production term $P_{i\theta}$, whereas for lower Prandtl numbers the dissipation term $\varepsilon_{i\theta}$ mainly balances the production due to the mean flow. This may be one of the reasons, why most proposals from literature are mainly focussing on an appropriate modelling of the pressure-scrambling term $\phi_{i\theta}$ or $\Pi_{i\theta}$. Furthermore, only simple formulations for the dissipation rate $\varepsilon_{i\theta}$, which assume a vanishing value of the latter quantity in the core region of the flow, are incorporated. Therefore, in the present investigation, only proposals are investigated, which especially take into account the increasing or decreasing importance of these two budget terms in consideration of the molecular Prandtl number Pr .

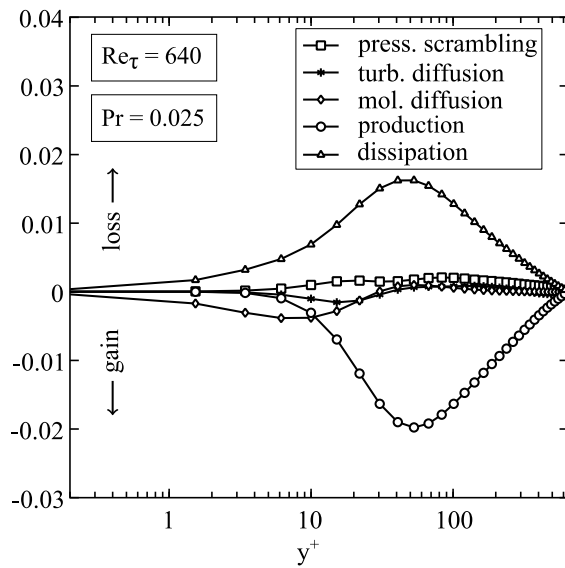


Figure 1. Analysis of the budget terms for a symmetrically heated planar channel flow and a molecular Prandtl number of $Pr = 0.025$ based on the DNS data of Abe et al. [4].

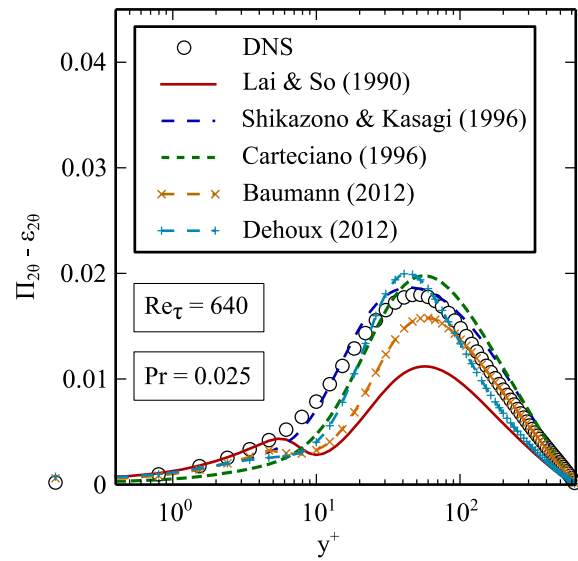


Figure 2. Comparison of different proposals for the difference of the pressure-scrambling $\Pi_{i\theta}$ and dissipation term $\varepsilon_{i\theta}$ based on the DNS data of Abe et al. [4].

As illustrated in Figure 2 for the wall-normal turbulent heat flux component, the best agreement for the prediction of the two budget terms can be achieved by the proposal of Shikazono & Kasagi [5]. One major disadvantage of this model is its limitation to rather simple channel flows, because the formulation of the correlation term $\Pi_{i\theta}$ is not frame invariant to rotation of the coordinate system. Therefore, it cannot be applied to complex geometries or flow types, e.g. square duct flows [5]. The model by Carteciano [6] introduces an additional term in the transport equations of the turbulent heat fluxes, which accounts for the effect of an increasing or decreasing importance of both of the budget terms in dependence of the Prandtl number Pr or turbulent Péclet number Pe_t , respectively. One shortcoming of this model is its violation of the asymptotic wall limiting behavior, which can be derived by a Taylor expansion series of the fluctuating quantities. This may be the result of its intended purpose; the numerical simulation of a hot sodium jet in different convection regimes [6]. The approach by Baumann [7] introduces rather empirical damping functions for both budget terms in dependence of the dimensionless wall-distance or the Prandtl number. It is thus not expected to be valid for a wide range of flow types. Dehoux [8] proposed a model for both budget terms based on the elliptic blending strategy, first published by Manceau & Hanjalić [9]. The model gives an acceptable agreement with the DNS data, but requires the user input of the time scale ratio in the homogeneous

region of the flow (R_h). This value is usually not known a priori for more complex geometries and flow types considering buoyancy effects.

Due to its simplicity in comparison with the other proposals, the model by Carteciano [6] is selected for further investigations. The combination of a full second-moment closure in buoyancy-dominated flows for the turbulent Reynolds stresses and the turbulent heat fluxes requires at least the solution of 16 differential equations. For that reason, a further reduction of the numerical model by algebraic truncation is considered.

2.2. Derivation of a new algebraic turbulent heat flux model

For the derivation of a new algebraic turbulent heat flux model, several simplifications and assumptions have to be considered, which will only be briefly presented in this paper. The interested reader is referred to the work of Dol et al. [10] for a detailed discussion of the validity of the latter assumptions in buoyancy-dominated flows.

The first assumption is the so-called weak-equilibrium hypothesis, which is based on the formulation of a dimensionless anisotropic heat flux vector ζ_i , and implicates that the latter quantity is constant in space and time:

$$\zeta_i = \frac{\overline{u_i \theta}}{\sqrt{k} \sqrt{\overline{\theta'^2}}}, \quad \text{and} \quad \frac{\mathbf{D} \zeta_i}{\mathbf{D} t} - D_{\zeta_i} = 0. \quad (2)$$

The origin of this assumption can be traced to the work of Rodi [11], which discusses the truncation of the transport equation of the anisotropy of turbulent Reynolds stresses. The convective and diffusive transport can be expressed by means of the transport terms of the turbulent kinetic energy k and of the temperature variance ($\overline{\theta'^2}$):

$$\frac{1}{\sqrt{k} \sqrt{\overline{\theta'^2}}} \left(\frac{\mathbf{D} \overline{u_i \theta}}{\mathbf{D} t} - D_{i\theta} \right) = \frac{1}{2} \left[\frac{\overline{u_i \theta}}{k^{3/2} \sqrt{\overline{\theta'^2}}} \left(\frac{\mathbf{D} k}{\mathbf{D} t} - D_k \right) + \frac{\overline{u_i \theta}}{\overline{\theta'^2}^{3/2} \sqrt{k}} \left(\frac{\mathbf{D} \overline{\theta'^2}}{\mathbf{D} t} - D_{\theta\theta} \right) \right]. \quad (3)$$

In fully developed flows it is obvious, that the sum of the total diffusion of the turbulent kinetic energy and the temperature variance equals the following expression:

$$D_{i\theta} = \frac{1}{2} \overline{u_i \theta} (D_k + D_{\theta\theta}). \quad (4)$$

By introduction of the budget terms the formulation in equation (4) can be further modified to:

$$P_{i\theta} + G_{i\theta} + \Pi_{i\theta} - \varepsilon_{i\theta} - \frac{\overline{u_i \theta}}{2k} (P_k + G_k - \varepsilon) - \frac{\overline{u_i \theta}}{2\overline{\theta'^2}} (P_{\theta\theta} - \varepsilon_{\theta\theta}), \quad (5)$$

where $P_{i\theta}$, P_k and $P_{\theta\theta}$ represent the production terms, $G_{i\theta}$ and G_k the production due to buoyancy forces, $D_{i\theta}$, D_k and $D_{\theta\theta}$ the total diffusion terms and $\varepsilon_{i\theta}$, ε and $\varepsilon_{\theta\theta}$ the dissipation terms of the turbulent heat fluxes $\overline{u_i \theta}$, the turbulent kinetic energy k and the temperature variance $\overline{\theta'^2}$, respectively.

Assuming an equilibrium of the production and dissipation terms of the two latter quantities can further reduce this formulation:

$$P_k + G_k = \varepsilon, \quad \text{and} \quad P_{\theta\theta} = \varepsilon_{\theta\theta}. \quad (6)$$

The remaining production term $P_{i\theta}$ is exact and needs no further modelling. For the modelling of the pressure scrambling $\Pi_{i\theta}$ and dissipation term $\varepsilon_{i\theta}$ any model of the literature can be used. In the present investigation, a slightly modified version of the model by Carteciano [6] is used. A careful recalibration of the coefficients and the removal of the wall-reflection term, see Lai & So [11] for a detailed discussion of its necessity, leads to the following models for both budget terms:

$$\Pi_{i\theta} = -C_{1\theta} \frac{\varepsilon}{k} \overline{u_i \theta} + C_{2\theta} \overline{u_j \theta} \frac{\partial \overline{U_i}}{\partial x_j} + C_{3\theta} \beta g_i \overline{\theta^2}, \quad (7)$$

$$\varepsilon_{i\theta} = \frac{1+Pr}{2\sqrt{Pr}\sqrt{R}} \exp(-C_{5\theta}(Re_t+Pe_t)), \quad (8)$$

where the turbulent Reynolds and Péclet numbers are given by $Re_t = k^2/(\nu\varepsilon)$ and $Pe_t = Pr Re_t$. The time scale ratio $R = \tau_{th}/\tau_m$ represents the ratio of the thermal time scale $\tau_{th} = \overline{\theta^2}/\varepsilon_{\theta\theta}$ and the mechanical time scale $\tau_m = k/\varepsilon$. For the present investigation, the two-equation model by So & Sommer [13] is used to calculate the time scale ratio R , which is validated for a wide range of molecular Prandtl numbers.

The final truncated algebraic heat flux model is therefore, given by the following expression:

$$\overline{u_i \theta} = -\left(\frac{k}{\varepsilon}\right) \frac{\overline{u_i u_j} \frac{\partial \overline{\Theta}}{\partial x_j} + \alpha \overline{u_j \theta} \frac{\partial \overline{U_i}}{\partial x_j} + \gamma \beta g_i \overline{\theta^2}}{C_{1\theta} + \frac{1+Pr}{2\sqrt{Pr}\sqrt{R}} \exp(-C_{5\theta}(Re_t+Pe_t))}, \quad (9)$$

where the parameters are given by $\alpha = (1 - C_{2\theta})$ and $\gamma = (1 - C_{3\theta})$. The complete set of coefficients of the present model is denoted in Table 1.

The present algebraic model is implicit in its formulation, which may result in numerical instabilities. Because the present simulations could be performed without any incident, the analysis of potential instabilities is postponed to further investigations. The present model is combined with a full second-moment closure for the turbulent Reynolds stresses based on the elliptic blending approach (RSM-EBM) by Dehoux [8]. This model is validated successfully for turbulent planar channel flows in different convection regimes.

Table 1. Coefficients of the present model.

Coefficient	Value
$C_{1\theta}$	3.6
$C_{2\theta}$	0.5
$C_{3\theta}$	0.5
$C_{4\theta}$	0.0
$C_{5\theta}$	0.0007/0.001

3. Results

3.1. Turbulent planar channel flow

The present algebraic model (AHM) is compared with available DNS and LES data of a turbulent channel flow from the literature [4],[14] at different Reynolds numbers Re_τ and at a molecular Prandtl number of $Pr = 0.025$. To analyze the influence of the coefficient for the dissipation term $\varepsilon_{i\theta}$, two slightly different values are investigated $C_{5\theta}=0.0007$ and $C_{5\theta}=0.001$.

As depicted in Figure 3 and Figure 4, the present AHM exhibits a nearly perfect agreement in case of the dimensionless temperature profiles with the DNS data by Abe et al. [4] for different Re_τ . The results for both values of the coefficients are almost identical and only a slightly better prediction may be stated for $C_{5\theta}=0.001$. One of the most essential requirements for turbulent heat flux closures is an appropriate prediction of the Nusselt number Nu , which can be formulated as:

$$Nu = \frac{2\delta \dot{q}_w}{\lambda (\bar{\Theta}_B - \bar{\Theta}_w)}, \quad (10)$$

where δ represents the half channel height, \dot{q}_w the heat flux applied on the walls, λ the thermal conductivity and $(\bar{\Theta}_B - \bar{\Theta}_w)$ the difference between the bulk and wall temperature. An investigation of the Nusselt number is especially useful, because most design tools of large-scale facilities use this integral quantity, which allows depicting the global system performance in transient operational scenarios by means of one-dimensional analysis of the heat transfer. For the present algebraic model, a close agreement with the DNS and LES [4],[14] data over a wide range of bulk Reynolds numbers Re_b and bulk Péclet numbers $Pe_b = Pr Re_b$, respectively, is observed. The deviations are in the range of 10%.

Analyzing several flow quantities, the AHM exhibits the most satisfying agreement. Therefore, in a next step in the validation process, this model is applied to geometries that are more complex.

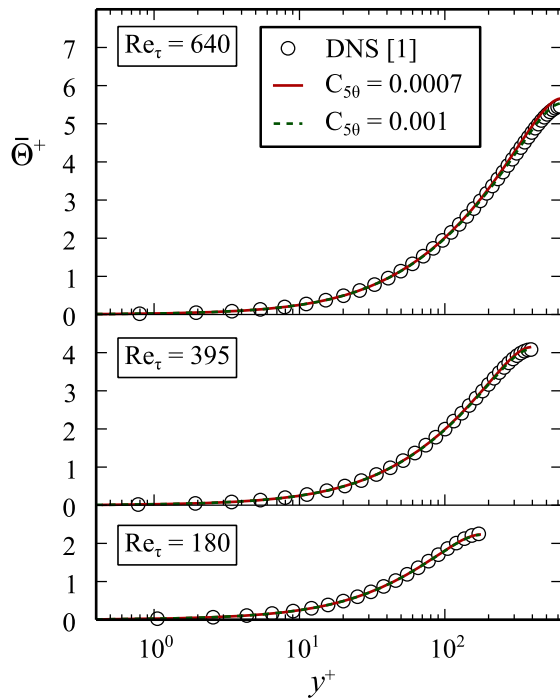


Figure 3. Dimensionless temperature profiles for the present AHM in comparison with the DNS data [4] at different Re_τ and $Pr = 0.025$.

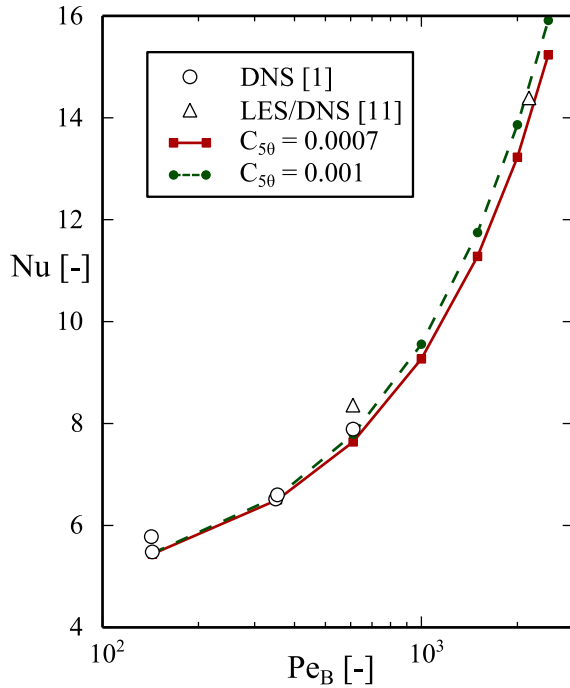


Figure 4. Comparison of the predicted Nusselt numbers for an increasing bulk Péclet number in comparison with DNS and LES data [4],[14].

3.2. Turbulent square duct flow

One of the main features of turbulent square duct flow is the intrinsic presence of secondary motions of the second kind, which are induced by differences in the turbulent normal and shear stresses. To the knowledge of the authors, presently no DNS data exists to investigate the turbulent heat transfer of liquid metals in turbulent square duct flows. Therefore, LES simulations are performed for different heating conditions and in different convection regimes. The results shown refer to a configuration for a constant, identical heating on one wall pair, whereas the other wall pair are assumed perfectly thermal insulating; see Figure 5. The molecular Prandtl and bulk Reynolds number are fixed at $Pr = 0.025$ and $Re_b = 7000$.

Figure 6 illustrates the results of the dimensionless velocity profiles of the LES and the RSM-EBM. It shows an acceptable agreement with the experimental data of Kawahara et al. [15] and the DNS data of Pinelli et al. [16]. Only a slight underestimation of the maximum of the velocity component in the cross-sectional plane is observed for the RANS approach. One major concern in the numerical model for liquid metal flows is the choice of a suitable domain size. As pointed out by Grötzbach [17] the largest turbulent structures are expected to occur in the temperature field. Therefore, it must be ensured that the domain size is sufficiently large to analyze the two-point correlations. The size of the domain and important parameters for the LES are given in Table 2.

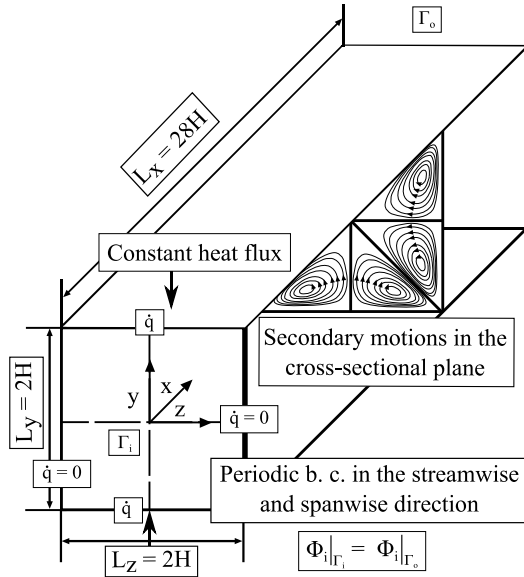


Figure 5. Sketch of the computation domain and definition of boundary conditions for the investigated turbulent square duct flow.

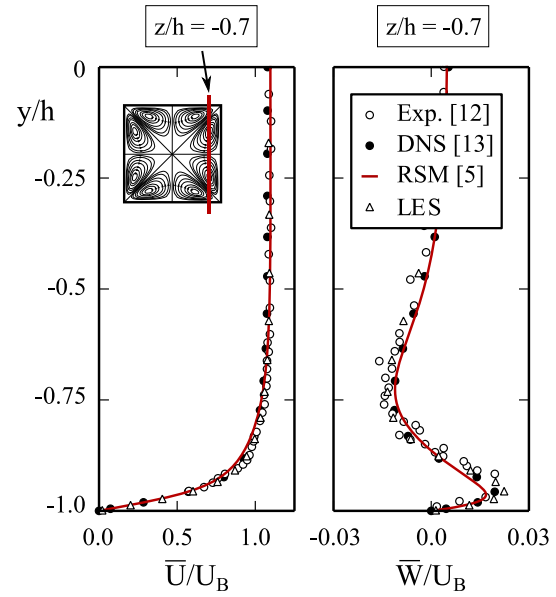


Figure 6. Comparison of the profiles of the streamwise and cross-sectional velocity component with exp. and DNS data [15],[16].

Table 2. Data sheet for the present LES.

Parameter	Symbol	Value
Bulk Reynolds number	$Re_b = U_b 2H/\nu$	7000
Mol. Prandtl number	Pr	0.025
Length of the domain	L_x	28H
Size of the cross-section	$L_y = L_z$	2H
No. of elements	$N_x \times N_y \times N_z$	245 x 120 x 120
Sampling time	$T_s U_b/H$	~8000
Spatial discretization	-	2 nd order
SGS- model	-	Dynamic Smagorinsky
SGS-heat flux model	$Pr_{t,SGS}$	∞

For an acceptable resolution of the velocity field, one can assume a nearly full resolution of the temperature field for low molecular Prandtl numbers [17]. Therefore, the results of the present algebraic heat flux model can be compared with the results of the LES.

The dimensionless temperature profile $\bar{\theta}^+$ is formulated based on the wall temperature at the wall bisectors $\bar{\theta}_{wb}$ and the mean friction velocity averaged over the walls $\langle u_\tau \rangle$:

$$\bar{\Theta}^+ = \frac{(\bar{\Theta}_{wb} - \bar{\Theta})}{T_\tau}, \quad \text{with} \quad T_\tau = \frac{\dot{q}_w}{\rho c_p \langle u_\tau \rangle}. \quad (11)$$

where ρ and c_p represent the density and the specific heat capacity of the fluid, respectively.

This setup of the numerical model represents a limiting case of non-vanishing temperature fluctuations on the walls, which is opposite to the limiting case of zero wall temperature fluctuations in the planar channel flow. In reality, the magnitude of the fluctuations of the temperature field is largely dependent on the thermal activity ratio, describing the ratio between the thermal properties of the solid and fluid. Due to the unknown distribution of the temperature variance at the surface, a zero value is assumed for the AHM, which is also adopted by other researchers [18],[19].

Both, in terms of the dimensionless temperature and the turbulent heat flux, see Figure 7 and Figure 8, the results of the present AHM are in a good agreement with the LES data. The dimensionless temperature in the centre of the square duct is slightly underestimated by the present AHM. This can be related to a slight overestimation of the turbulent heat flux component in the y-direction of the duct. Due to the higher contribution of turbulence to the total heat fluxes, hot fluid is penetrating deeper into the core region of the duct.

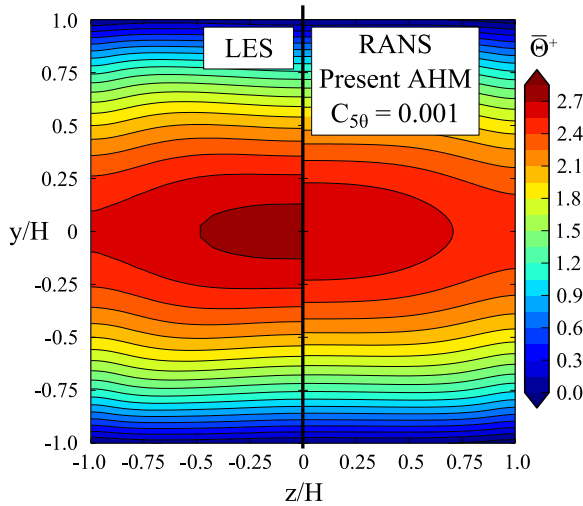


Figure 7. Comparison of the dimensionless temperature distribution in the cross-sectional plane of the duct.

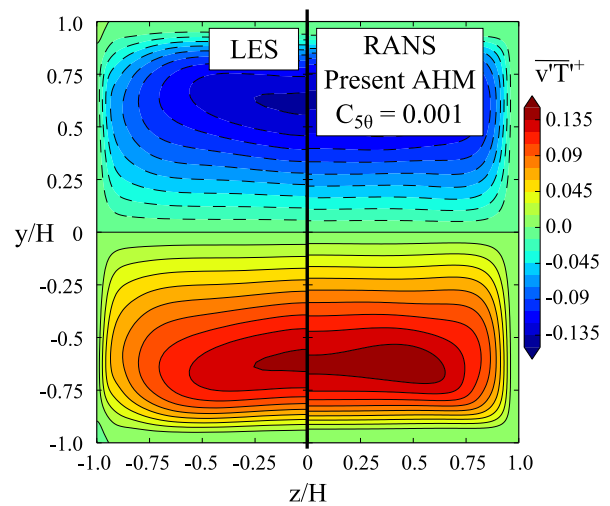


Figure 8. Comparison of the dimensionless turbulent heat flux in the cross-sectional plane of the duct.

To investigate the performance of the model within the mixed convection regime, additional LES for a fully developed square duct flow are performed at a Richardson number $Ri = 0.09$:

$$Ri = \frac{Gr}{Re_b^2} = \frac{\beta \cdot g \cdot \dot{q}_w \cdot 2H^2}{\lambda \cdot u_b^2}, \quad (12)$$

with

$$Gr = \frac{\beta \cdot g \cdot \dot{q}_w \cdot \rho^2 \cdot 2H^4}{\lambda \cdot \eta^2}, \quad (13)$$

where β represents the volumetric expansion coefficient, \dot{q}_w the heat flux on the solid wall, H the wall distance, λ the thermal conductivity and u_b the bulk velocity.

Only the wall at the bottom is heated and all three other walls are assumed perfect thermally insulated. The gravity force g_i is applied in the streamwise directions. The size of the computational domain corresponds to that of the forced convective flow case.

As can be seen in Figure 9 the agreement between both simulations is acceptable for the streamwise velocity component even though the curvature of the isotachs into the corners is slightly underrated by the RANS approach. The magnitude of the secondary motions \bar{S}/u_b is smaller for the RANS approach compared to the LES (see Figure 10), which can be referred to the underlying Reynolds stress model (RSM-EBM). Because secondary flow motion is a direct consequence of an appropriate prediction of the turbulent normal and shear stresses, further improvements should focus on the influence of buoyancy effects within the framework of the elliptic blending procedure.

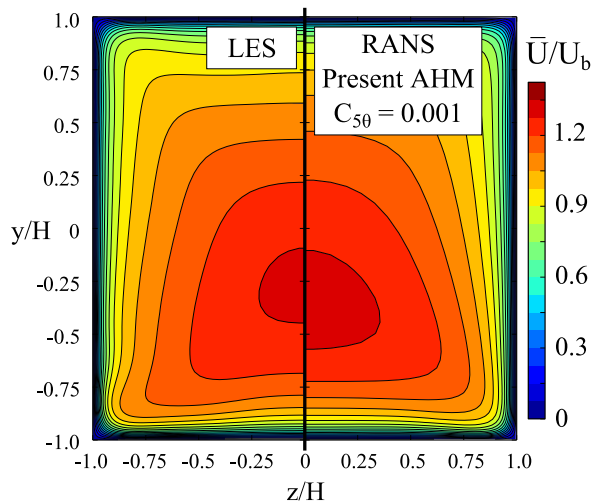


Figure 9. Comparison of the dimensionless streamwise velocity distribution in the cross-sectional plane of the duct.

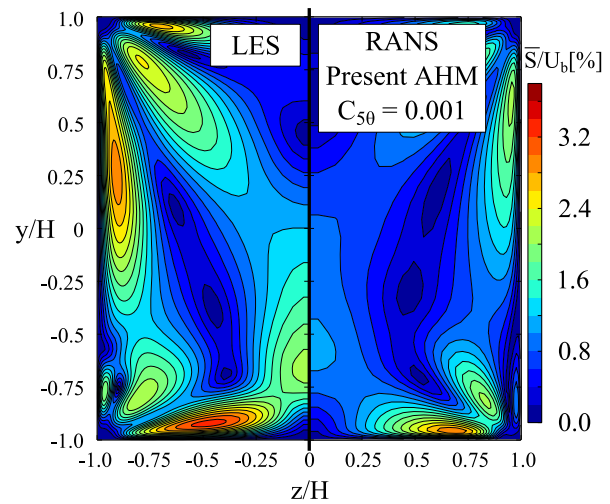


Figure 10. Comparison of the dimensionless magnitude of secondary motion in the cross-sectional plane of the duct.

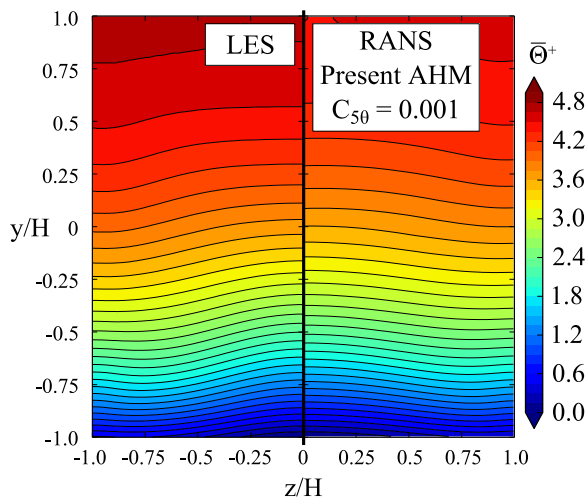


Figure 11. Comparison of the dimensionless temperature distribution in the cross-sectional plane of the duct.

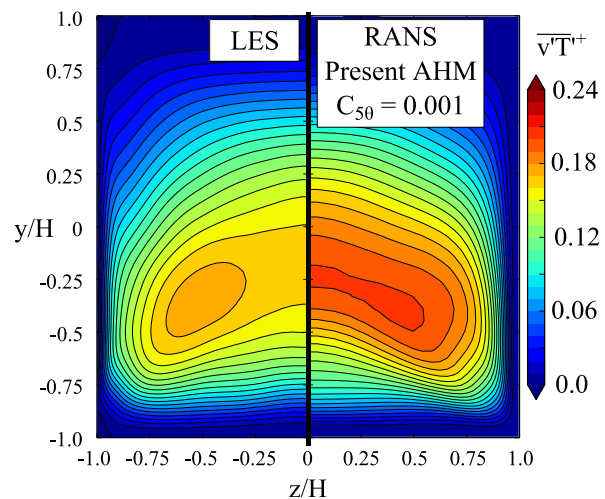


Figure 12. Comparison of the dimensionless turbulent heat flux in the y-direction within the cross-sectional plane of the duct.

With respect to the predicted dimensionless temperature profile the agreement is nearly perfect (see Figure 11) with only a minor deviations (underestimation) near the insulated wall at the top. Due to a slightly overestimation of the turbulent heat flux component in the y-direction of the AHM (see Figure 12), the dimensionless temperature profile is slightly shifted from the bottom to the top of the duct in comparison with the LES results.

As listed in Table 3 the AHM shows a close agreement with the LES for the Nusselt number in both convection regimes.

Table 3. Comparison of the predicted Nusselt numbers

Type	Heating condition	Ri [-]	Nu [-]
LES	symm.	0	5.91
RANS	symm.	0	5.86
LES	asymm.	0.09	3.75
RANS	asymm.	0.09	3.76

4. Direct Numerical Simulations

Very recently, Direct Numerical simulations of the laterally heated flow in a vertical square duct could be accomplished at TU Dresden. The Navier-Stokes equations with Boussinesq approximation have been solved using a Finite-Volume method of second order on staggered grids together with a Runge-Kutta scheme of second order in time [20][21]. Here, the reference length $H^* = L_y = L_z$ is used for normalization and definition of similarity numbers. The length of the channel is assumed to $L_x = 24H^*$ and no-slip conditions are imposed at the walls. For the dimensionless over-temperature $\theta = (T - T_b)/\Delta T$, Dirichlet conditions $\theta(y = 0) = 1$ and $\theta(y = H) = 0$ are considered together with an adiabatic condition on the remaining sidewalls. The grid consists of $1024 \times 166 \times 166$ cells, being uniform in x-direction, with the same distribution in y- and z-direction including refinement close to the walls. This grid resolves all the turbulent scales with the first grid point at the wall located at $y_1^+ < 0.4$.

Simulations are conducted for $Re_b^* = U_b H^* / \nu = 6200$, and $Ri^* = 0$ as well as $Ri^* = 0.1$ assuming liquid sodium with $Pr = 0.0088$, which is lower than the value used above. Averaging has been performed in time over about $1500H^*/U_b$ and $1600H^*/U_b$, respectively, as well as in x-direction, and the symmetry of the solution with respect to the plane $z/H = 0.5$ has been exploited for an additional averaging step. Simulation results in case of forced convection have been validated with the data of Ma et al. [22].

Figure 13 and 14 provide information on the mean streamwise flow (top row) as well as the secondary flow in the cross plane (second row). These latter show the magnitude of the secondary flow, termed u_\perp here, in terms of a contour plot as well as the corresponding streamlines of the secondary flow. It is obvious that under the prevailing conditions the pattern is substantially altered with respect to $Ri=0$. The graphs in the third row show the temperature which is very smooth, similar to Figure 11 above and which drives the axial flow on the left-hand side, i.e. close to $y=0$, upwards. As a result, the flow is accelerated near the hot wall and decelerated near the cold wall. Furthermore, the pattern of the secondary flow is substantially altered, with a pair of two vortices near the hot wall and a smaller pair near the cold wall and the stagnation point shifted towards the cold wall. The changes of the secondary flow pattern result from altered balances of the individual Reynolds stress components. The secondary flow transporting hot fluid towards the cold wall in the channel center creates enhanced fluctuations near the cold wall so that the turbulent kinetic energy is substantially increased in this region. The cross-plane turbulent heat fluxes are visualized in the last row with the color scale determined by the magnitude of this vector. It is visible that this quantity is larger by a factor of more than 3 and exhibits a pattern similar to the kinetic energy.

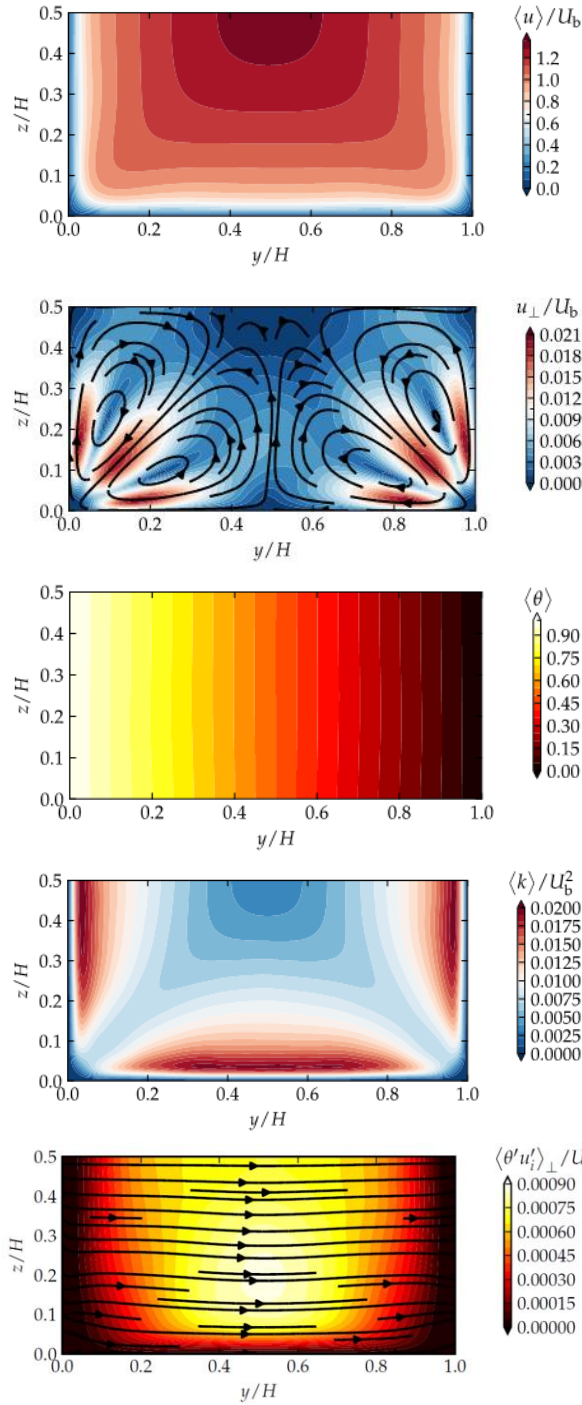


Figure 13. Mean streamwise velocity, secondary flow, temperature, turbulent kinetic energy, and cross-plane turbulent heat flux for $Ri^* = 0$, i.e. forced convection.

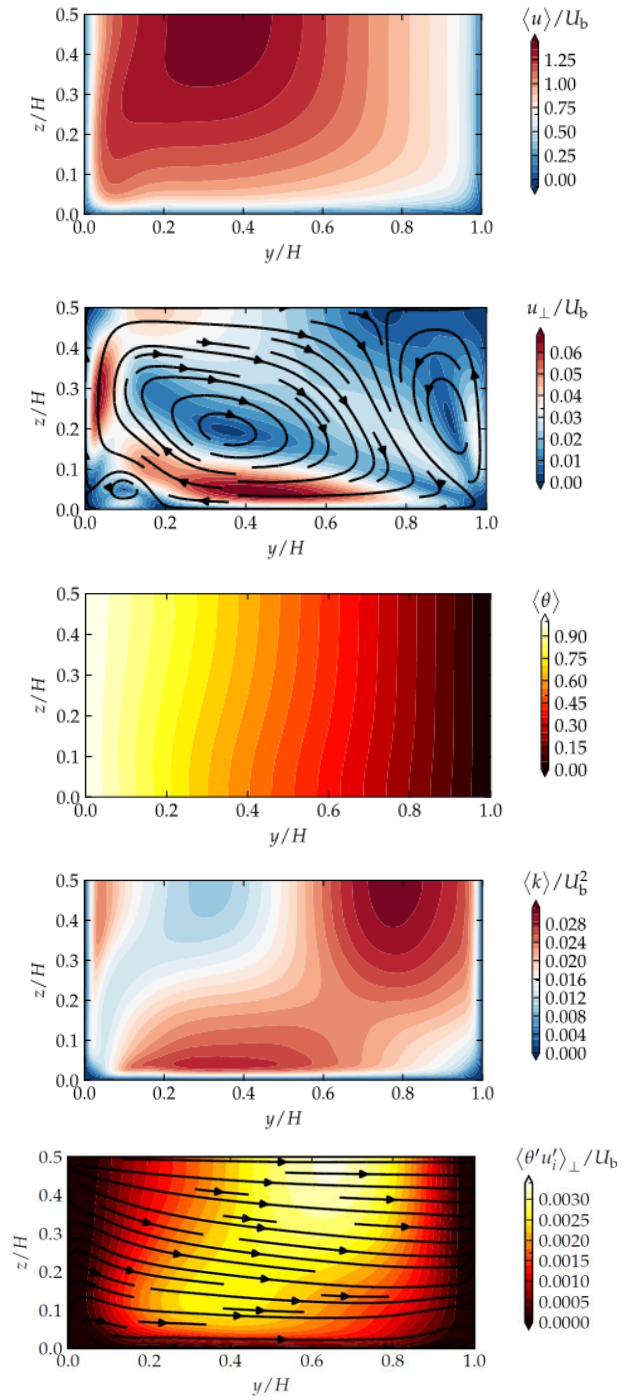


Figure 14. Mean streamwise velocity, secondary flow, temperature, turbulent kinetic energy, and cross-plane turbulent heat flux for $Ri^* = 0.1$ (the color scales adapted in case of different range).

From the DNS just described, all Reynolds stresses were determined, as well as all terms in their budget equations. These are now available for further analysis and can be used in modeling activities.

More evaluations and additional simulations with $Ri^*=0.02$ and $Ri^*=0.5$, together with LES for $Re_b^*=40000$ and $Ri^*=0, 0.02$, and 0.1 , will be the subject of subsequent investigations.

5. Comparison with experimental results

The above presented modelling approach and results exhibits one of the drawback related to CFD code modelling – the presence of a validated reference solution. Reference solution can be either obtained by quasi-exact direct numerical solutions or high resolution experimental data. But, the number of available and high quality experiments is rather sparse. Furthermore, these experiments are mainly related to forced convection, although a large fractions shows unintended buoyancy support. In Jaeger et al. [23] experiments are listed, which focus on quadratic and rectangular flow geometries operated with liquid metals. Mostly those studies provide empirical correlations for the Nusselt number as a function of the Péclet number, which are valid for rectangular ducts with an aspect ratio of less than 10 (width over depth) and for parallel plate-like ducts with an aspect ratio of larger or equal to 10. In addition, the available data for wall drag coefficients are compared to common friction factor correlations. It is shown that correlations for pipe flow conditions are applicable to quadratic and rectangular channel flows. These results are compared in Jaeger et al. [24] with results generated by turbulence models for RANS CFD in a benchmark.

For the benchmark, a rectangular duct with an aspect ratio of 10 is selected (width = 250 mm, depth = 25 mm). For the sake of completeness, DNS data from Kawamura for a parallel plate geometry are added to the comparison. The results for the Nusselt number and the wall drag coefficient are depicted in Figure 15 and Figure 16.

The benchmark shows, that a rectangular duct with an aspect ratio of 10 is very similar to a parallel plate, indicated by the similar results of the DNS data and all other data. The secondary motions caused by the corners lose their importance with increasing aspect ratio. From an engineering point of view, the differences between the modelling approaches are marginal. In the same way, the wall drag coefficients predicted with empirical models, RANS CFD and DNS show almost identical results.

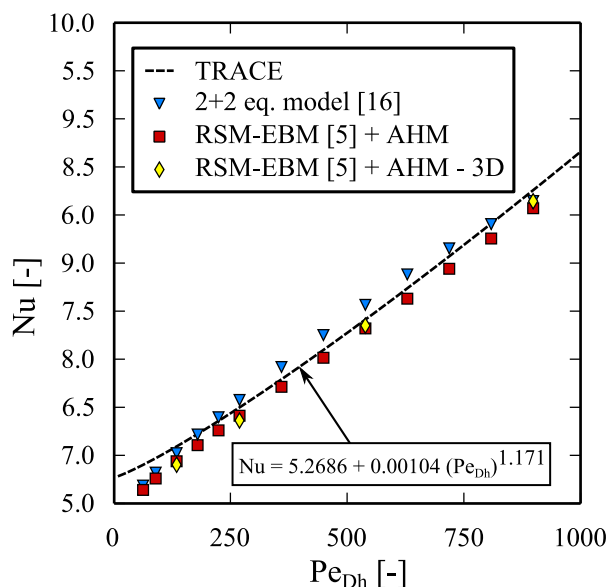


Figure 15. Comparison of numerical results originating from different modelling approaches for the heat transfer under forced convection.

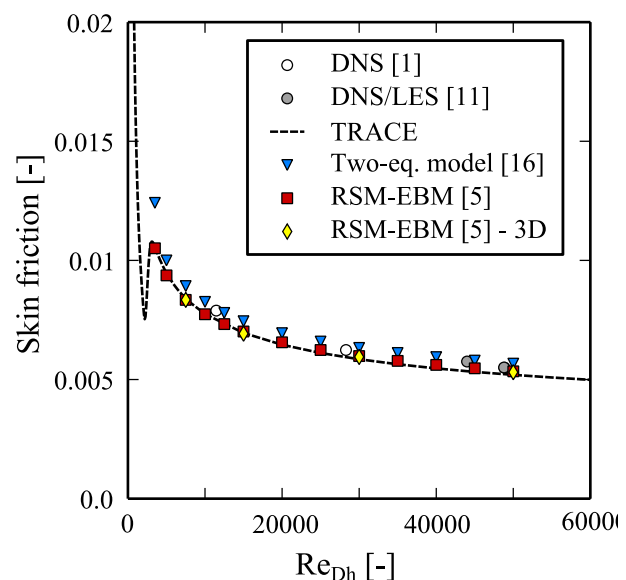


Figure 16. Comparison of numerical results originating from different modelling approaches for the wall drag coefficient under forced convection.

Even though the comparison of empirical models derived from and developed for experiments and the results generated with CFD and DNS codes shows identical qualitative trends and similar quantitative values, a conclusive statement concerning the prediction capabilities of numerical codes cannot be made.

The only way to proof the validity of the used models and approaches, for both empirical models and turbulent heat flux models, is by a direct comparison with experimental data. Therefore, experiments are under construction and currently in assemblage at the Institute for Neutron Physics and Reactor Technology at the KIT.

The first experiment foreseen is a rectangular flow channel with an aspect ratio of two. This rectangular duct will be integrated into the KASOLA facility. This duct consists of a 3600 mm long commercially available duct. The internal dimensions of this duct are 90 mm in width and 40 mm in depth. A detailed description of the KASOLA facility may be taken from [25].

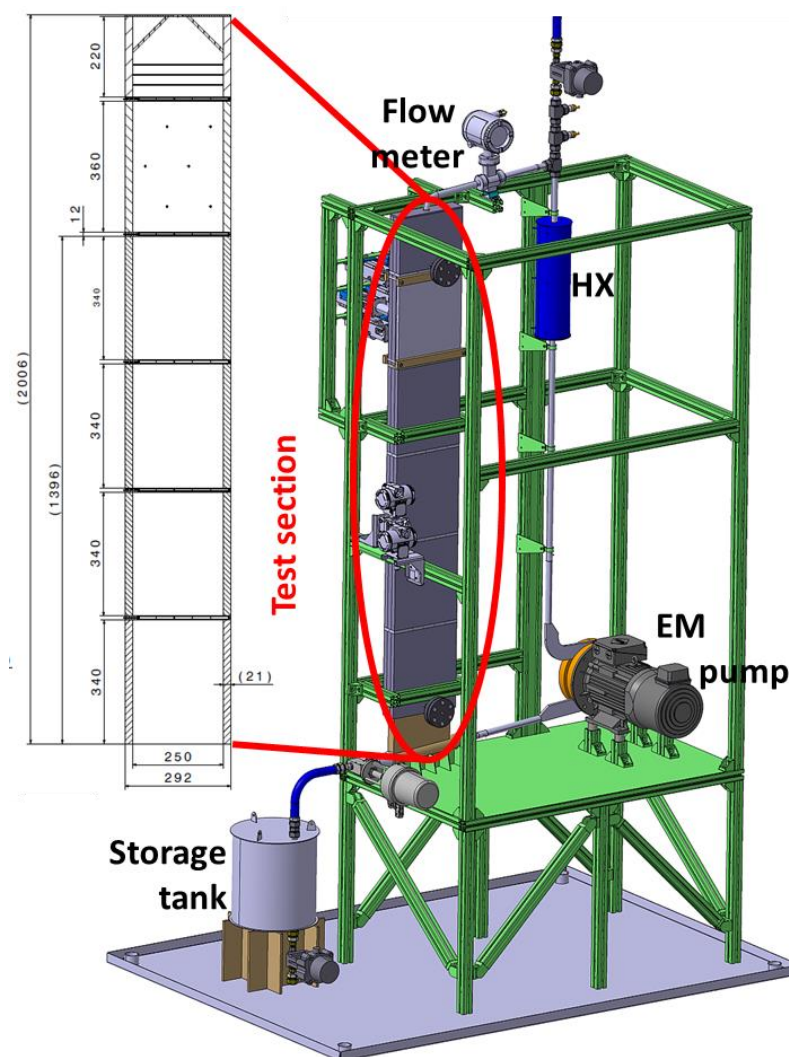


Figure 17. Experimental loop (right side) of the proposed experiment.

In the above presented turbulent heat flux modelling approach, the issue of the secondary motions due to the corners is introduced. The comparison of experiments with larger aspect ratios showed that for aspect ratios of 10 and more the influence of the secondary motions can be neglected. Therefore, the second experiment will investigate the flow and heat transfer in a rectangular duct with an aspect

ratio of 10. Due to the design of the KASOLA facility, ducts with larger aspect ratios cannot be installed. Therefore, the second experiment is integrated in a new loop, being operated with the eutectic Gallium- Indium-Tin alloy. Due to its low melting point, $< 11^\circ\text{C}$, the expenditures are reasonable low. The schematic arrangement of the experimental set-up is depicted in Figure 17. The main components of the experimental loop are: the rectangular test section, a flow meter, a heat exchanger and a pump.

The flow meter is commercial inductive flow meter. The heat exchanger is of the shell-and-tube counter current flow type with InGaSn in the tube and water in the shell. This heat exchanger is connected to a commercial chiller unit. The pump is an electromagnetic one basically consisting of a motor with two discs placed next to the flow channel. The two discs are equipped with permanent magnets. The motor rotates the discs and by means of the Lorentz force the electrically conducting InGaSn is accelerated. Furthermore, the loop contains of a storage tank and several valves, pressure taps, thermo-couples, etc. for operation and control of the experimental loop.

The realization of the test section itself is shown in Figure 18. The test section is basically a rectangular channel with an aspect ratio (width- $2W$ to depth- H) and internal flow dimensions of $250\text{ mm} \times 25\text{ mm}$. The test section is 2000 mm long and over the whole length, 85 thermo-couples are installed at five different levels (17 per level). At each level, the thermo-couples are arranged in measurement crosses to obtain temperature data over the whole width and depth. The levels of these crosses are indicated in Figure 18 by means of red lines. They are located at the positions $x/H = 25, 50, 75, 100$ and 125 composed of a set of sensors located at the fluid wall interface, at $y/H = 0.25, 0.5$ and 0.75 and $z/2W = 0.0, 0.5$ and equidistant spaced in transverse.

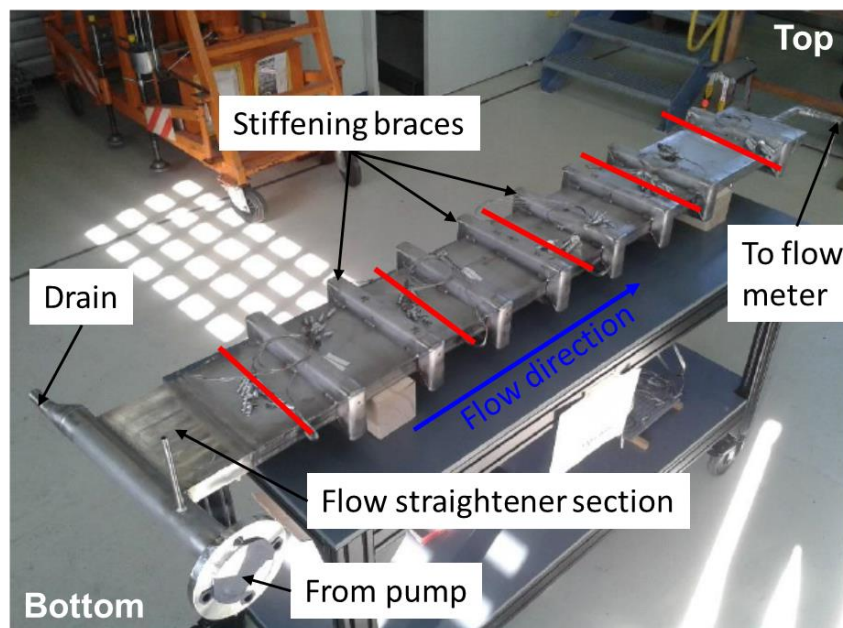


Figure 18. Rectangular test section of the experimental loop.

To investigate the heat transfer behavior under transitional behavior (forced convection to mixed convection to free convection) a heating plate is used, which is attached to the flow channel on one outside of the wall of the rectangular channel. The heating plate covers the entire width $2W$ of the flow channel, and is equipped with standard resistance heating wires, capable to provide up to 400 W per installed meter. With a total length of 8200 mm the heater can produce up to 3280 W , which corresponds to a mean heat flux of $q = 26\text{ kW/m}^2$ applied to the channel wall over a length of $x/H = 20$. The entire section is thermally insulated by rockwool with a heat conductivity of $38\text{ mW/(m}\cdot\text{K)}$ to limit the thermal losses. The test section is supplied fluid flow by means of a MHD pump with a

pressure difference of $\Delta p = 2$ bar, providing a maximum flow of 1 l/s. By this set-up a Reynolds number of up to $Re = 15000$ and Richardson number of up to $Ri = 0.4$ can be achieved covering a large range of technical interest.

For the heat removal, a counter current shell and tube design heat exchanger is installed at the top of the loop. The inner pipe is the downward pipe of the loop piping. The shell side envelops this pipe. On the shell side, water is cooling the heated Indium-Gallium-Tin alloy. This heat exchanger is connected to a commercial cooler system.

6. Summary

This article addresses the vital engineering challenge to reliably predict the heat removal from a heated wall by liquid metals in different flow regimes, as they occur naturally during start-up/shut-down of pumps, normal operational transients etc. Accurate temperature and flow predictions using conventional numerical tools necessitate modified turbulence models to take the peculiarities of liquid metals into account. In this context, a new algebraic turbulent heat flux model for low molecular Prandtl number flows has been derived and carefully analysis in terms of the budget terms and algebraic truncation of the turbulent heat flux equations. In a first step this model is validated for turbulent channel flows and exhibits only marginal deviations to available DNS and LES data from the literature. In a second step the performance of the model is studied for a turbulent square duct flow at moderate Reynolds numbers. In the absence of DNS or LES data for liquid metal flows, an LES-simulation within forced and mixed convection regime has been set-up to derive a data set for mandatory to serve as model validation. The present algebraic model shows in this benchmark exercise a satisfactory agreement with the LES data, especially within the forced convection regime. Due to the high complexity of the equations, when the temperature acts as an active scalar contributing to the buoyancy terms, the RANS approach shows still an acceptable agreement with the LES results but deviations are increasing.

In further investigation the influence of the underlying thermal two-equation model will be evaluated. Additionally, LES for several different heating conditions and Prandtl numbers have to be executed to analyse this impact on the budget terms and to judge more completely on the capabilities of the model. Only then a holistic assessment of the present approach in comparison with other turbulent heat flux models from the literature can be made.

The ultimate proof of validity will be given only after a comprehensive code to experiment comparison. Therefore, two different experimental campaigns are under development to provide experimental data to obtain, among others, Nusselt numbers during different convection schemes and the transition among them.

Acknowledgments

The financial support of the Helmholtz Alliance “Liquid Metal Technologies – LIMTECH” is gratefully acknowledged.

References

- [1] Pacio J 2015, Low Prandtl number thermal-hydraulics, pp. 647-730 in OECD, Handbook on Lead-bismuth Eutectic Alloy and Lead Properties, Materials Compatibility, Thermal-hydraulics and Technologies, NEA No. **7268**
- [2] Wetzel T 2015, Instrumentation, pp. 731-839 in OECD, Handbook on Lead-bismuth Eutectic Alloy and Lead Properties, Materials Compatibility, Thermal-hydraulics and Technologies, NEA No. **7268**
- [3] Onea A, Perez-Martin S, Jaeger W, Hering W and Stieglitz R 2017, Liquid metals as heat transfer fluids for science and technology pp. 305-376 in Minea A A (Ed.), Advances in new heat transfer fluids, CRC Press
- [4] Abe H, Kawamura H and Matsuo Y 2004 *Int. J. Heat and Fluid Flow* **25** 404-19

- [5] Shikazono N and Kasagi N 1996 *Int. J. Heat Mass Transfer* **39** 2977-87
- [6] Carteciano L N 1996 *Wissenschaftliche Berichte FZKA* **5775**
- [7] Baumann T 2012, *Ph.D Thesis Karlsruhe Institute of Technology (KIT)*
- [8] Dehoux F 2012 *Ph.D thesis SIMMEA Université de Poitiers*
- [9] Manceau R and Hanjalić K 2002 *Phys. Fluids* **14** 744-54
- [10] Dol H S, Hanjalić K and Kenjereš S 1997 *Int. J. Heat Fluid Flow* **18** 4-14
- [11] Rodi W 1976 *Zeitschrift für angewandte Mathematik und Mechanik* **65** 219-21
- [12] Lai Y G and So R M C 1990 *Int. J. Heat Mass Transfer* **33** 1429-40
- [13] So R M C and Sommer T P 1994 *Trans. ASME*. **116** 844-54
- [14] Duponcheel M, Bricteux L, Manconi M, Winckelmans G and Bartosiewicz Y 2014 *Int. J. Heat Mass Transfer*. **75** 470-82
- [15] Kawahara G, Ayukawa K, Ochi J, Ono F and Kamada F 2000 *Trans. JSME B* **66** 95-102
- [16] Pinelli A, Uhlmann M, Sekimoto A and Kawahara G 2010 *J. Fluid Mech.* **644** 107-22
- [17] Grötzbach G 2011 *Nucl. Eng. Des.* **241** 4370-90
- [18] Sommer T P, So R M C and Zhang H S 1994 *J. Heat Transfer* **116** 855-63
- [19] Manservigi S and Menghini F 2014 *Nucl. Eng. Des.* **273** 251-70
- [20] Kempe T, Fröhlich J 2012 *J. Comput. Phys.* **231** 3663–3684
- [21] Niemann M, Fröhlich J 2016 *Int. J. Heat Mass Transfer* **101** 1237–1250
- [22] Ma L-D, Li Z-Y, Tao W-Q 2007 *Heat Mass Transfer* **44** 229–250.
- [23] Jaeger W, Hering W, Lux M and Portes F 2015 *Proc. Int. Conf. on Nuclear Engineering*, Chiba, Japan, May 17-21
- [24] Jaeger W, Trimborn F, Hering W, Pritz B and Gabi M 2016 *Proc. Int. Congr. on Advances in Nuclear Power Plants*, San Francisco, April 17-20
- [25] Jaeger W, Hering W, Stieglitz R Schum T, Frohnepfel B, Niemann M and Fröhlich J 2017 *IOP Conf. Ser.: Mater. Sci. Eng.* (this volume)